Examining high-resolution survey methods for monitoring cliff erosion at an operational scale

Pauline Letortu, Marion Jaud, Philippe Grandjean, Jérôme Ammann, Stéphane Costa, Olivier Maquaire, Robert Davidson, Nicolas Le Dantec, Christophe Delacourt

1 **Examining high-resolution survey methods for monitoring cliff erosion**

2 **at an operational scale**

3 Pauline Letortu[a*], Marion Jaud[b], Philippe Grandjean[c], Jérôme Ammann[b],

4 Stéphane Costa[d], Olivier Maquaire[d], Robert Davidson[d], Nicolas Le

5 Dantec[b,e], Christophe Delacourt[b]

6 [a]*University of Bretagne Occidentale, CNRS, UMR LETG, IUEM, Rue Dumont d'Urville,*

7 *Plouzané, 29280, France; tel: +33 290915588; pauline.letortu@univ-brest.fr*

8 [b]*University of Bretagne Occidentale, CNRS, UMR Géosciences Océan, IUEM, rue*

9 *Dumont d'Urville, Plouzané, 29280, France; tel: +33 298498710*

10 [c]*University of Lyon 1, CNRS, UMR Sciences de la Terre, 2 rue Raphaël Dubois,*

11 *Bâtiment GEODE, Villeurbanne, 69622, France; tel: +33 472728499*

12 [d]*Normandie Univ, UNICAEN, CNRS, UMR LETG, Esplanade de la Paix, Caen, 14000,*

13 *France; tel +33 231565141*

14 [e]*CEREMA - Cerema, Direction Eau Mer et Fleuves, 134 Rue de Beauvais, Margny-lès-*

15 *Compiègne, 60280, France*

16

17 **Examining high resolution survey methods for monitoring cliff erosion**

18 **at an operational scale**

19   This paper aims to compare models from terrestrial laser scanning (TLS),

20   terrestrial photogrammetry (TP), and unmanned aerial vehicle photogrammetry

21   (UAVP) surveys to evaluate their potential in cliff erosion monitoring. TLS has

22   commonly been used to monitor cliff-face erosion (monitoring since 2010 in

23   Normandy) because it guarantees results of high precision. Due to some

24   uncertainties and limitations of TLS, TP and UAVP can be seen as alternative

25   methods. First, the texture quality of the photogrammetry models is better than

26   that of TLS which could be useful for analysis and interpretation. Second, a

27   comparison between the TLS model and UAV or TP models shows that the mean

28   error value is mainly from 0.013 to 0.03 m, which meets the precision

29   requirements for monitoring cliff erosion by rock falls and debris falls. However,

30   TP is more sensitive to roughness than UAVP, which increases the data standard

31   deviation. Thus, UAVP appears to be more reliable in our study and provides a

32   larger spatial coverage, enabling a larger cliff-face section to be monitored with a

33   regular resolution. Nevertheless, the method remains dependent on the weather

34   conditions and the number of operators is not reduced. Third, even though UAVP

35   has more advantages than TP, the methods could be interchangeable when no

36   pilot is available, when weather conditions are bad or when high reactivity is

37   needed.

38   Keywords: Coastal cliff erosion; monitoring; terrestrial laser scanning; terrestrial

39   photogrammetry; UAV photogrammetry; Normandy

40   **1 Introduction**

41 Changes to coastal cliffs are complex because of the sudden and stochastic natures of

42 erosion in time and place and the diversity of movements (rock falls and debris falls

43 according to the typology of Varnes). Despite contributions to research into

44 geomorphological processes on rocky coasts in recent years, the respective contribution

45 of the triggering factors responsible for erosion is still difficult to determine (Naylor et

46 al. 2010; Lim et al. 2011; Letortu et al. 2015a; Laute et al. 2017).

47   As quantifying changes in unstable and subvertical cliff face is difficult and

48   sometimes dangerous, in situ data are mainly collected by remote-sensing methods.

49   Data with a horizontal or quasi-horizontal point of view (side scanning a vertical

50   structure as the cliff face) allow all changes to be observed because the data capture cliff

51   face changes which reflect failures and deposits anywhere on the cliff profile (contrary

52   to cliff top and cliff base). High spatial resolution and high temporal repetitiveness are

53   essential to reveal patterns of cliff failure (location, time) and therefore to better

54   understand and forecast the processes responsible for cliff erosion (e.g. Collins and Sitar

55   2008; Hampton 2002; Vann Jones et al. 2015; Young 2015).

56   Different methods terrestrial Laser Scanning (TLS), Aerial Laser Scanning

57   (ALS), Mobile Laser Scanning, Unmanned Aerial Vehicle Photogrammetry (UAVP),

58   Terrestrial Photogrammetry (TP) are available for cliff monitoring depending on the

59   precision, the spatial and temporal scales, and costs (e.g., Young et al. 2010; James and

60   Robson 2012; Michoud et al. 2014). As reported in James and Robson (2012), for

61   restricted areas (ranges of 10–500s of meters) terrestrial laser scanners or TP can be

62   used. Over larger areas, aerial photogrammetry, aerial laser scanners, and space-based

63   radar and photogrammetric techniques are possible.

64   Within the framework of the "Service National d'Observation DYNALIT"

65   (French National Service Observation for the study of coastal and coastline dynamics),

66   we survey the cliff-face evolution in Petit Ailly site in Varengeville-sur-Mer

67   (Normandy, France) to quantify fine-scale changes, to visualize the modalities of

68   evolution and to contribute to the debate about the agents responsible for the retreat of

69   the chalk cliffs. Since October 2010, a 3D monitoring of the cliff face has been

70   performed by terrestrial laser scanner (an active remote-sensing instrument) at very high

71   spatial resolution and with pluricentimeter precision ($\pm$ 0.03 m) every 3-4 months

72   (Letortu et al. 2015b). It enables reliable, homogeneous, frequent and perennial

73   monitoring of rock falls and debris falls. However, the TLS routine is expensive and

74   cumbersome and therefore requires several operators. UAVP and TP surveys may be

75   efficient alternatives offering data of equivalent quality.

76   Is the accuracy of close-range techniques, such as TP and UAVP, sufficient in

77   comparison with the more expensive and cumbersome TLS routine for monitoring cliff-

78   face erosion? The answer to this question involves many topics: (1) the resolution

79   and/or ground sampling distance (2) the spatial coverage (3) the accuracy and precision

80   of the datasets for diachronic surveys of individual and mass movements, and (4) an

81   easy-to-use acquisition protocol for the site configuration and data processing. If the

82   different techniques achieve the same level of data quality, these methods could be

83   interchangeable, depending on weather conditions and people availability, without any

84   impact on the monitoring results.

85   Thus, this article presents an original comparison for such environment of three

86   high-resolution remote-sensing methods implemented for 28 January 2016: (1)

87   measurement by TLS and two photogrammetric methods based on Structure from

88   Motion/Multi-View Stereophotogrammetry (SfM-MVS) techniques from (2) UAV

89   photographs and (3) terrestrial photographs. After a brief description of the study area,

90   this paper details the survey methodology. Finally, the results of the cliff-face

91   monitoring are presented and discussed.

92   **2 Study area**

93   The study takes place near Dieppe, in Seine-Maritime (Normandy) in the northwestern

94   part of France and along the Channel. Geologically, the Upper Normandy coastal cliffs

95   (60-70 m high on average) extending from Cap d'Antifer to Le Tréport (100 km) are

4

96   made of various chalk with flints of Upper Cretaceous (Pomerol et al. 1987; Mortimore

97   and Duperret 2004). The different stages of chalk (from the oldest to the newest:

98   Cenomanian, Turonian, Coniacian, Santonian and Campanian) present slight variations

99   in facies and fine sedimentary discontinuities, inducing some subtle resistance contrasts.

100 Over these chalk strata, the usual residual flint formation (Laignel 1997; Costa et al.

101 2006) have been replaced by a bed of clay and sand sediments about 10-30 m thick of

102 Paleogene age (Bignot 1962), especially in Sainte-Marguerite-sur-Mer, Varengeville-

103 sur-Mer, and Sotteville-sur-Mer (Figure 1). The Seine-Maritime cliff coast is

104 characterized by the regressive dynamics, coming out as instantaneous falls affecting all

105 or part of the cliff. A monitoring of the regressive dynamics of the cliff top between

106 1966 and 2008 shows a retreat rate of 0.15 m/year with high spatial variability in Upper

107 Normandy (Letortu et al. 2014).

108 The SNO DYNALIT site of Petit Ailly is located along Cap d'Ailly

109 (https://www.dynalit.fr/fr/falaises/ailly-puys). More precisely, it lies on either side of

110 the Petit Ailly dry valley in Varengeville-sur-Mer (Figure 2). This site is made up of

111 Santonian chalk, covered by a bed of clay and sand of Paleogene age, prone to erosion.

112 It has a high erosion rates calculated from TLS surveys: from October 2010 to June

113 2017, the erosion rate is 0.38 m/year with a fallen volume of 12965 m^3 ($\pm$155 m^3) due to

114 rock falls and debris falls. Nevertheless, these average retreat rates are not

115 representative of the erosion which occurs suddenly caused by rockfalls. For example,

116 in February 2014, a rock fall of approximately 5000 m^3 resulted in a cliff-top retreat of

117 11 m in a few seconds.

118   The studied cliff face is characterized by (1) its verticality (from 70° to

119 overhang); (2) its height (about 30-40 m); (3) its spatial extent (250 m long); (4) debris

120 falls, which are individual movements of blocks or flakes (up to decimeters), and rock

121 falls, which describe large-scale mass movements from all or part of the cliff face; and

122 (5) its limited accessibility (rock falls, tide constraints, difficulty in setting up targets at

123 the cliff top).

124 **3 Methods**

125 *3.1 Data collection*

126 *3.1.1 Terrestrial laser scanner data collection and ground control points*

127 A terrestrial laser scanner is an optical active remote-sensing technology that can

128 measure the position (distance and angle) of a point relative to the device using the time

129 of flight of laser pulses reflected by the point to be measured.

130 The instrument used in this study is a Riegl® VZ-400 (Figure 2(6)) emitting a

131 laser pulse in the near-infrared (1550 nm), which records unique echo digitization but

132 allows the digitized echo-signals (waveform data) to be processed in Riegl® software.

133 This instrument provides scan data acquisition with theoretical 0.005 m accuracy and

134 0.003 m precision at a range of 100 m. The measurement range can reach up to 600 m

135 while the measurement rate can reach up to 122,000 measurements per second with a

136 wide field of view of 100° vertical (from 30° to 130°) and 360° horizontal (Riegl 2014).

137 Moreover, the Riegl® VZ-400 is equipped with a Nikon D800 camera, which provides

138 photographs. These pictures can be used to drape a 2D image on the 3D point cloud but

139 are not an absolute requirement for topographic measurement. In Varengeville-sur-Mer,

140 the two scanner stations are positioned on the beach at about 75 m from the cliff face.

141 TLS acquisition involves a 360° horizontal and 100° vertical scan with an angular

142 resolution of 0.04° in both directions, providing a dense 3D point cloud (more than 22.5

143 million points) and five photographs in 9 min (20 % overlap by default). These

144 instruments are heavy, 20 kg for the scanner and 1 kg for the Nikon camera, and require

145 complementary equipment (a tripod, cases, batteries, targets and a total station).

146 To carry out georeferencing and obtain repeated surveys of high accuracy, the

147 data acquisition process requires additional equipment: reflective targets (10cm high

148 cylinders, 0.15 kg, Figure 2(4)) used as ground control points (GCPs) and a total station

149 to measure them (Figure 2(2)). Contrary to the GPS, the total station measures points

150 close to the cliff front without a mask effect. The Trimble M3 total station is precisely

151 positioned at a single location previously known by raw data GPS post-processing.

152 Knowing the reflective targets absolute coordinates enables the point cloud acquired in

153 a relative coordinate system to be projected in an absolute coordinate system (Lambert

154 93 and associated RGF93 and IGN69, official reference system in France; EPSG:

155 2154). For the TLS survey at Petit Ailly, laser scans were performed from two stations

156 with 15 targets as GCPs (Figure 3). To reduce the alignment error of the point cloud,

157 targets are numerous and with different distances from the scanner (as long as they all

158 remain visible).

159 *3.1.2 Terrestrial photo collection*

160 Terrestrial photographs are acquired with a Nikon D800 reflex camera (1 kg) with a

161 focal length of 35 mm, taking 36 Mpix photos. To collect data on the cliff front, as

162 recommended by James and Robson (2012), images of the area of interest are acquired

163 from different positions. As depicted in Figure 5a, the camera orientations are not

164 parallel but rather converge on the scene. The procedure to collect digital photographs is

165 quite easy to implement. It involves short distances between the acquisition positions

166 (around 2–3 m when taking photos at ∼20 m from the cliff foot) and photos taken at

167 angular intervals of 10–20°, over a wide range of angles. To obtain a high-quality

168 dataset, photographs should overlap by at least 60 % (ideally, a point should be seen at

169 least three times) and must capture the area with at least two shooting angles. In 23 min,

170 the whole cliff section (250 m long) was covered by a dataset of 153 photographs

171 collected along the baseline depicted in Figure 3. The overlap enables that any point in

172 the studied cliff face being present in six to more than nine photographs.

173 *3.1.3 UAV photo collection*

174 The drone survey is implemented using an electric hexacopter UAV, called DRELIO 10

175 (multi-rotor DS6 platform assembled by DroneSys). A collapsible frame enables it to be

176 folded for easy transportation. With a 0.8m diameter, the DRELIO 10 weighs less than

177 4 kg and can handle a payload of 1.6 kg. The flying time is about 20 min. On a tilting

178 gyro-stabilized platform, a Nikon D800 reflex camera with a focal length of 35 mm is

179 set up. The camera takes 36 Mpix photographs in intervalometer mode every 2 s. The

180 DJI® software iOSD runs the flight control. For delicate steps of the take-off and

181 landing, the pilot prefers to control the UAV thanks to ground station software.

182   The dataset is collected along the yellow baseline depicted in Figure 3. As

183 shown in Figure 5b, data at the cliff top were collected by the camera that is in the nadir

184 position. To collect data on the cliff front, the camera was forward-pointed and tilted at

185 25°. In this case, the flight has to be performed in manual mode to keep the camera

186 turned toward the cliff face. The flight lasted around 8 min. In this configuration, the

187 dataset is composed of 110 oblique and nadir images (that will be processed together),

188 any point in the studied cliff face being present at least in 9 photographs.

189 *3.1.4 GCPs for TP and UAVP*

190 Like the TLS survey, TP and UAVP need GCPs (targets) to record the models in a

191 reference coordinate system and to achieve models of the highest quality, in terms of

8

192   both geometrical precision and georeferencing accuracy. The absolute coordinates are

193   provided by additional equipment : the total station (previously described). In order to

194   obtain a high-quality final model (James and Robson 2012) and help to mitigate doming

195   effects caused by an incorrect camera model and radial distortion (James and Robson

196   2014), a large number of GCPs is recommended. The GCPs need to be distributed

197   throughout the area of interest (Javernick et al. 2014; Smith et al. 2014) without linear

198   configurations. They should ideally cover both the margins and the center of the area of

199   interest, with a good range of values in each spatial dimension. However, in a cliff

200   context, access to the cliff face is dangerous due to frequent rock falls. It can therefore

201   be difficult to ensure targets are clearly visible while guaranteeing the safety of the

202   person installing them at the top of the cliff. The lack of targets on the upper part of the

203   cliff face may create distortion. To avoid this concern, the photograph acquisition

204   protocol was implemented cautiously. The UAV camera was forward-pointed and tilted

205   at 25° with photographs at different distances from the cliff face to reduce distortion.

206   For TP, a great variety of viewing angles of terrestrial photographs was taken to limit

207   the doming effect (Jaud et al. 2017b). A total of 17 targets were used for TP with

208   different configurations: 9 were vertically positioned on the area of interest (center of

209   orange crosses, 40 cm high, painted on the lower part of the cliff face, Figure 2(5))

210   while 8 targets (circular disks, 23 cm in diameter, Figure 2.1) were horizontally

211   positioned on the beach (Figure 3). For UAVP, 22 targets (circular disks, 23 cm in

212   diameter, Figure 2(1)) were horizontally positioned on the beach, on the lower part of

213   the valley slope and on the cliff top (Figure 3).

214   ***3.2 Data processing***

215   *3.2.1 Terrestrial laser data processing and absolute error quantification*

216   The main steps in the TLS data processing are (1) georeferencing and point cloud

217   assembly (RiscanPRO® software); (2) manual point cloud filtering including areas

218   without overlap with previous TLS data, noise and vegetation (Fledermaus®); and (3)

219   Delaunay 2.5D meshing (best fit plane, Cloudcompare®).

220   The scanning survey of each position is recorded as a 3D point cloud (x,y,z) in a

221   reference system relative to each position of the scanner in the field. The accuracy of

222   georeferencing is carried out by comparing the position of the control points in the

223   model with the GCPs precisely measured on the field using the Root Mean Square Error

224   method (measuring the differences between values predicted by a model and the values

225   really observed) (Kaiser et al. 2014; Eltner et al. 2016). This accuracy assessment is

226   only valid if the point cloud is considered consistent (distortion due to atmospheric

227   effects is neglected). For the first and second stations, the standard deviations of fit

228   residues are 0.0091 and 0.0093 m, respectively. The absolute error on the data

229   (accuracy) is the sum of the TLS instrumental errors, the total station measurement

230   errors, and topographic inaccuracies during georeferencing. The theoretical instrument

231   accuracy of the TLS is very high ($\pm$ 0.005 m at a range of 100 m), so the main source of

232   error comes from the total station survey, which measures the target positions with

233   accuracy from 0.01 to 0.03 m.

234   In a context of recurrent TLS surveys, a procedure of accuracy assessment has

235   been implemented. It is based on the comparison of the position of 3 fixed points

236   (surveyor nails located on the descending road to the sea) measured by the total station

237   during the 18 successive missions carried out within the framework of the DYNALIT

238   observatory. The 6 July 2011 topographical survey is defined as a reference because the

10

239   survey conditions were optimal. Identified thanks to their dispersion from the reference

240   data, the poor measurements are removed. The validated data have a maximum

241   dispersion ellipse of 0.018 m in x, 0.019 m in y and 0.033 m in z (Figure 4).

242   For diachronic comparisons to quantify local erosion rates, the point clouds are

243   adjusted relative to this point cloud of reference (6 July 2011) using a best fit algorithm.

244   To keep the consistency of this protocol, the comparison between TLS data and

245   photogrammetric data is also based on a best fit adjustment.

246   *3.2.2 Photograph data processing and precision*

247   The procedure for deriving 3D point clouds from photographs is based on the SfM-

248   MVS workflow. The SfM-MVS algorithm is implemented by AgiSoft® PhotoScan

249   Professional (version 1.2) (Figure 5). The positions of the GCPs are imported into

250   Agisoft® PhotoScan and, concurrently, the GCPs are pointed out on the photographs to

251   compute the georeferenced 3D point cloud.

252   The 3D surface reconstruction is divided into two main steps:

253   • Camera alignment by bundle adjustment. Tie points are detected and matched on

254   overlapping photographs so as to compute the external camera parameters

255   (position and orientation) for each picture. From 17 to 22 GCPs (targets located

256   on the cliff front and on the beach for TP; targets on the beach for UAVP) are

257   tagged to georeference data and refine the internal parameters of the camera.

258   • From the estimated camera positions and the pictures themselves,

259   stereophotogrammetric equations allow the software to compute the position of

260   each tie point, so as to build a dense point cloud.

261   There is no direct measurement of accuracy from TP or UAVP because the

262   surveyor nails (fixed in a horizontal position) are not always visible in these datasets.

263   TLS data are considered the reference dataset for comparison in this paper, so, as

264   previously mentioned, TP and UAVP point clouds have been fitted to TLS data.

265   Therefore, the measure of precision of the photogrammetric reconstruction for TP and

266   UAVP datasets is assessed relative to the synchronous TLS dataset. The best fit RMS

267   error is of 0.04 m between TP and TLS and UAVP and TLS.

268   *3.3 Data comparison*

269   First of all, TLS and photogrammetric methods (UAVP and TP) differ in the nature of

270   collected data and so resulting products. The main advantage of UAVP and TP is that

271   they provide textured models of better quality than the TLS model. When scanning a

272   site, by default, the TLS takes only five photographs for a 360° horizontal angle (with

273   an overlap of 20%). This is not enough to create, from all angles, a textured model

274   taking into account the terrain (Figure 6b). It is possible to increase the overlap but

275   because of fixed points of view of TLS stations, it would be hard to match the

276   photogrammetric model. In fact, the process of SfM-MVS itself involves the use of

277   ten(s) of high-resolution photographs, thus enabling the algorithm to choose perfectly

278   the relevant photographs to texture each parcel of the model (Medjkane et al. accepted).

279   It thus constitutes an important asset for the morphological analysis and interpretation

280   of landscapes (Figure 6c and d).

281   A first comparison of raw data is provided in Table 1. For the TP dataset,

282   because the photographs were taken closer to the cliff face than for the other datasets,

283   more photographs were needed to cover the area of interest so the sampling distance on

284   the cliff face was greater than for UAVP (Table 1). The volume of data was so large

285 that it was not manageable; it had to be processed in chunks. The steps for a more

286 advanced quantitative comparison were

287 (1) Cleaning the point cloud around the cliff face to obtain a good surface overlap;

288 (2) Subsampling TP and UAVP datasets to obtain manageable ones. The distance

289   sampling was a point every 0.06 m to have the same mean sampling as the TLS

290   point cloud, considered the reference;

291 (3) Fitting TP or UAVP models to the TLS point cloud used as the reference with

292   Cloudcompare and 3DReshaper software; and

293 (4) Comparison of the subsampled fitted point clouds (TP_SF, UAVP_SF) with the

294   TLS mesh (2.5D Delaunay mesh).

295   After dataset subsampling (0.06 m) of TP and UAVP models, quick filtering

296 around the cliff face and the beach and a fitting between TP or UAVP models and the

297 reference data (i.e. the TLS point cloud), the final point clouds can be quantitatively

298 compared (Table 2).

299   As in many papers (Westoby et al. 2012; Kaiser et al. 2014; Eltner et al. 2015;

300 Smith et al. 2016), we consider TLS models as the reference although they may also

301 have bias. As declared by Kromer et al. (2015), "the ability to detect change by

302 comparing a series of point clouds is controlled by the point cloud accuracy, precision,

303 survey design and terrain factors." For the TLS point cloud, these parameters are, as

304 Kromer et al. (2015) point out:

305   the scanner target distance (Teza et al. 2007), vegetation (Su and Bork 2006),
306   incidence angle (Sturzenegger and Stead 2009; Lato et al. 2010; Pesci et al. 2011),
307   surface reflectance (Csanyi and Toth 2007), surface roughness (Lague et al. 2013),
308   atmospheric conditions (Beckmann 1965), heterogeneity in point spacing (Raber et
309   al. 2007), alignment error (Oppikofer et al. 2009) and instrument specifications
310   (Pirotti 2013). Some of these factors contribute to the random Gaussian point-to-

311   point noise (precision), and others contribute to a systematic error (Lichti and

312   Skaloud 2010).

313   However, we consider the TLS dataset the reference in this relative comparison

314 because (1) within the TLS dataset, measurement errors related to the accuracy of the

315 laser are constant (0.005 m at a range of 100 m) while errors inherent in georeferencing

316 are transmitted to the whole cloud; (2) vegetation is scarce on the cliff face; (3) the

317 incidence angle is close to the normal direction and so the noise and systematic error of

318 the TLS point cloud are likely to be low.

319   For a quantitative data comparison, four calculation algorithms can be used

320 (Kromer et al. 2015): (1) M3C2 (2) mesh to point or mesh to mesh change detection (3)

321 spatial filtering (with calibration) and (4) space-time filter (with calibration). We used

322 mesh (for the TLS dataset) to point (photogrammetry datasets) because (1) the spatial

323 distribution of density from TLS, TP, and UAVP is different leading to an

324 overassessment of the distance between points; (2) the shortest distance calculation

325 enables change in different directions to be interpreted; and (3) noise is reduced through

326 the creation of the mesh of TLS data.

327 **4 Results and discussion**

328 *4.1 Global quality assessment*

329 The characteristics of the resulting point clouds differ from one method to another

330 (Table 2). As shown in Figure 7:

331   • The spatial distribution of the density is highly variable within the TLS point

332   cloud due to the positions of the TLS stations. The most homogeneous densities

333   are unsurprisingly UAVP and TP not only because of subsampling but also

334   because of the modus operandi, with a moving point of view during data

335   collection. UAVP has the most homogeneous density due to the automatic

336   snapping every 2 s.

337   • The best spatial coverage is observed for the UAVP model with no occlusion.

338   With the subsampled fitted (SF) point clouds, the comparisons of TP_SF and

339 UAVP_SF datasets with the TLS dataset highlight the low error value (millimeter to

340 centimeter values), which is relevant to observe debris falls. The mean error value is

341 mainly from 0.013 m to 0.03 m (Figure 8c and d). However, artifacts on datasets have

342 values superior to 1 m. These artifacts could be partially due to the error-assessment

343 method overestimating the error when the point cloud density is drastically different

344 between the compared datasets (because of occlusion).

345   Over the whole datasets, the mean error value is of 0.005 m for the TP model,

346 whereas it is of 0.014 m for the UAVP one. Thus, the TP model is more precise than the

347 UAVP one relative to the TLS reference. Nevertheless, the standard deviation is lower

348 for the UAVP_SF model than for the TP_SF one, so the dispersion of the measurement

349 error is lower (Table 3). In our comparison, the most important issue is to have a low

350 measurement error dispersion in order to obtain a reliable dataset (Figure 8a and b), and

351 so, for this purpose, the UAVP dataset appears to be the most relevant.

352   During data acquisition, the three datasets may suffer from occlusion due to

353 terrain factors (rock falls, overhanging areas, hollow areas, vegetation, and caves).

354 Occlusion is minimized with the TP and UAVP surveys relative to the TLS surveys

355 because the SfM-MVS survey covered the whole cliff face thanks to a greater number

356 of points of view. The UAV flight provides the largest number of cliff-face views and

357 can avoid the concern about overhanging. With the TLS surveys, time limitations

358 determine the number of possible tripod set-ups meaning that gaps may occur in the

15

359   final point cloud owing to occlusion. In such a context, a small number of targets are an

360   important issue because decreasing the duration per station will improve the spatial

361   coverage and the accuracy of the TLS surveys (Jaud et al. 2017a).

362   *4.2 Local quality assessment*

363   In the previous data comparison, when a point in one dataset is situated in a zone

364   without data (due to occlusion) in the compared dataset, the point to mesh distance is

365   measured relative to the nearest point, introducing an overestimation of the error. To

366   avoid this, we defined strips of the cliff face (Figure 9) considered to be without

367   artifacts in the error assessment (without vegetation, rock falls, complex morphology,

368   occlusion, etc.).

369   First, for all cliff-face strips, both data comparisons give nearly the same mean

370   error (0.015 m for TP-TLS comparison and 0.016 m for UAVP-TLS comparison) and

371   standard deviation values (0.031 and 0.026 m, respectively, for TP-TLS and UAVP-

372   TLS comparisons). So, without occlusion, the results from both methods seem to be

373   comparable.

374   Second, the mean error values are similar between the whole cliff face and strips

375   for UAVP (0.014 and 0.015 m, respectively). The standard deviation is slightly lower

376   for the strips than for the whole cliff face (0.026 against 0.037 m) due to surface

377   homogeneity, which limits overestimation. For TP, the results are different. The mean

378   error value is higher for the strips than for the whole cliff face (0.016 and 0.005 m,

379   respectively), whereas the standard deviation is lower for the strips than for the whole

380   cliff face (0.031 and 0.05 m, respectively). This means that occlusion significantly

381   affects the TP results. UAVP appears to be a more reliable and stable method whichever

16

382 surface is studied (cliff-face morphology, vegetation, etc.) whereas TP is much more

383 sensitive to roughness.

384 *4.3 Elements for choosing a relevant survey method*

385 According to our results, the choice of a suitable method for cliff erosion monitoring

386 depends on many criteria that are summarized in Table 4.

387   The main advantages of TLS are the precision of the data and the low dispersion

388 due to the consistency of the dataset (including the georeferencing step). Another

389 advantage is the long battery life, which enables many surveys to be carried out,

390 especially if the distance between stations can be increased to cover a larger area and a

391 single target can be used per survey (visible from every TLS station). The main

392 disadvantages of TLS remain the very expensive purchase and maintenance costs and

393 the weight. TLS field campaigns have low ability to implement survey because the

394 stations have to be close to the area of interest and the instrument is heavy (50 kg

395 including instruments, cases, batteries, a tripod and targets) and cumbersome. Easy

396 access to the area is necessary. Moreover, the weather conditions are a restraining factor

397 (in addition to tide times) since the instrument is highly sensitive to rain, wind, and fog,

398 which may be frequent in coastal areas (Table 4). The alternative of a hand-held mobile

399 laser scanner, which has been recently used for cliff-erosion monitoring (James and

400 Quinton 2014), could overcome the portability concern but the purchase of new material

401 is not desirable.

402   The main strengths of TP are very long battery life, very low sensitivity to bad

403 weather, very good ability to implement survey, and low cost. Because this method

404 needs a light instrument, which has a low energy consumption, the survey can be done

405 with the highest battery life. Thanks to these major advantages, the survey can be highly

406   reactive and easily carried out before/during/after a morphogenesis event. The main

407   weaknesses are the dispersion of the data and the processing duration (Table 4).

408   The main strengths of UAVP are the modus operandi, which can be adapted to

409   the configuration of the study area (very high flexibility in the ability to capture the

410   interest area) and very high speed of data acquisition. With a UAV pilot, sites that are

411   difficult to access can be monitored since the take-off and landing can be in the

412   hinterland. With a suitable flight plan, the distance-to-target can be varied to avoid

413   occlusion due to topographic complexities (Abellan et al. 2016). However, having a

414   pilot available (a key skill) can be a major constraint and weather conditions have to be

415   dry, with neither strong wind nor fog. Mild weather conditions may be a limiting factor

416   in coastal zones. Moreover, as TP, the duration of data processing may be longer than

417   for the TLS data (Table 4).

418   In the context of the observatories, the camera network (photo or video) could

419   be a complementary approach. More precisely, this instrumentation would not be used

420   for a precise quantification of observed changes but seems more suitable for a site of a

421   hundred meters maximum to capture erosion events because of its higher temporal

422   resolution. In fact, the time sampling of the TLS, PT, and UAVP surveys does not

423   provide this kind of information. The precise time of the observed change is important

424   to constrain the driving forces and, if possible, identify the triggering factor. Moreover,

425   with this information, a quantification survey can be planned when necessary. Thus,

426   video monitoring, combined with the precise quantification of changes thanks to TLS,

427   UAVP or TP, could improve the understanding of the agents and processes responsible

428   for cliff erosion and failure forecast. However, deployments of video cameras are not

429   possible everywhere because of the site configuration. A camera network needs to be

18

430   installed on a fixed support (e.g., on large rocks that can protect cameras from waves,

431   spray and abrasion) with a suitable view angle (embayed coast).

432   Each of the techniques presented in this paper has different strengths and weaknesses.

433   The choice of the instrument(s) (it could be a combination) to carry out monitoring

434   depends on the required precision, the costs, the site configuration (accessibility, height,

435   danger, morphology, etc.), the time, the people and skills available, as well as the

436   weather conditions and legal framework (for UAV).

5 Conclusion

438   Because the precision of a centimeter range (mean error value from 0.013 to 0.03 m) is

439   reached by the TP and UAVP, these can be seen as complementary methods to TLS

440   cliff erosion monitoring in Normandy. However, it should be remembered that TP is

441   sensitive to roughness, which can increase the standard deviation of data. Moreover, in

442   order to obtain textured models of good quality, SfM-MVS models are clearly better

443   than those of TLS. Because the TLS survey is cumbersome and expensive, the lower

444   costs of TP or UAVP seem attractive. However, it is important to bear in mind that the

445   choice is specific to accuracy expectations; the site configuration (accessibility, height,

446   danger, morphology, etc.); the time available to do the survey; the people and skills

447   available; financial resources; weather conditions and the legal framework (for UAV).

448   For our cliff erosion survey, TLS remains a good option because the methodological

449   framework can be improved (e.g. a single target) but UAVP is an interesting alternative:

450   (1) with a large spatial coverage in a few minutes with numerous viewpoints that avoid

451   occlusion; (2) a lighter weight and a higher flexibility in the ability to capture interest

452   areas than TLS; and (3) easy site access because the take-off and landing can occur in

453   the hinterland. However, this method needs a qualified pilot and if the area of interest is

454 near sensitive stakes (houses, airports, etc.), it could take time to obtain the flight

455 authorization. Another main weakness is its high sensitivity to weather conditions

456 (especially wind and rainfall), which can delay many surveys in the coastal zone.

457 Therefore, if a reactive method is needed, TP could be a good option. Despite some

458 drawbacks, SfM-MVS has changed topographic data collection in a wide range of

459 environmental settings and should have a bright future because of technical

460 developments in the devices and software.

461

462 References

463 Abellan, A., Derron, M. H., and M. Jaboyedoff. 2016. "Use of 3D Point Clouds in
464   Geohazards. Special Issue: Current Challenges and Future Trends." *Remote*
465   *Sensing* 8 (130). doi:10.3390/rs8020130.

466 Beckmann, P. 1965. "Signal degeneration in laser beams propagated through a turbulent
467   atmosphere." *Journal of Research of National Bureau Standards. Sect. D: Radio*
468   *Science 69D*: 629-640.

469 Bignot, G. 1962. "Étude sédimentologique et micropaléontologique de l'Éocène du Cap
470   d'Ailly (près de Dieppe, Seine-Maritime)." PhD diss., University of Paris.

471 Collins, B. D., and N. Sitar. 2008. "Processes of coastal bluff erosion in weakly lithified
472   sands, Pacifica, California, USA." *Geomorphology* 97: 483-501.

473 Costa, S., Laignel, B., Hauchard, E., and D. Delahaye. 2006. "Facteurs de répartition
474   des entonnoirs de dissolution dans les craies du littoral du Nord-Ouest du Bassin
475   de Paris." *Zeitschrift für Geomorphologie* 50: 95-116.

476 Csanyi, N., and C. K. Toth. 2007. "Improvement of lidar data accuracy using lidar-
477   specific ground targets." *Photogrammetric Engineering & Remote Sensing* 73:
478   385–396.

479 Eltner, A., Baumgart, P., Maas, H. G., and D. Faust. 2015. "Multi-temporal UAV data
480   for automatic measurement of rill and interrill erosion on loess soil." *Earth*
481   *Surface Processes and Landforms* 40: 741-755.

482 Eltner, A., Schneider, D., and H. G. Maas. 2016. "Image-based surface reconstruction in
483   geomorphometry - merits, limits and developments." *Earth Surface Dynamics* 4:
484   359-389.

485   Hampton, M. 2002. "Gravitational failure of sea cliffs in weakly lithified sediment."
486   *Environmental and Engineering Geoscience* 8 (3): 175-191.

487   James, M. R., and J. N. Quinton. 2014. "Ultra-rapid topographic surveying for complex
488   environments: the hand-held mobile laser scanner (HMLS)." *Earth Surface*
489   *Processes and Landforms* 39: 138-142.

490   James, M. R., and S. Robson. 2012. "Straightforward reconstruction of 3D surfaces and
491   topography with a camera: accuracy and geoscience application." *Journal of*
492   *Geophysical Research: Earth Surface* 117: F03017. doi:
493   10.1029/2011JF002289.

494   James, M. R., and S. Robson. 2014. "Mitigating systematic error in topographic models
495   derived from UAV and ground-based image networks." *Earth Surface Processes*
496   *and Landforms* 39: 1413-1420. doi: 10.1002/esp.3609.

497   Jaud, M., Letortu, P., Augereau, E., Le Dantec, N., Beauverger, M., Cuq, V., Prunier,
498   C., Le Bivic, R., and C. Delacourt. 2017a. "Adequacy of pseudo-direct
499   georeferencing of terrestrial laser scanning data for coastal landscape surveying
500   against indirect georeferencing." *European Journal of Remote Sensing* 50 (1):
501   155-165.

502   Jaud, M., Passot, S., Allemand, P., Le Dantec, N., Grandjean, P., Ammann, J., and C.
503   Delacourt. 2017b. "Stratégies d'optimisation d'acquisition par drone pour
504   limiter les distorsions lors de la reconstruction 3D par les logiciels Photoscan et
505   MicMac." Poster presented at Journées CRITEX, Grenoble, May 10-12.

506   Javernick, L., Brasington, J., and B. Caruso. 2014. "Modelling the topography of
507   shallow braided rivers using Structure-from-Motion photogrammetry."
508   *Geomorphology* 213: 166-182. doi:10.1016/j.geomorph.2014.01.006.

509   Kaiser, A., Neugirg, F., Rock, G., Müller, C., Haas, F., Ries, J., and J. Schmidt. 2014.
510   "Small-scale surface reconstruction and volume calculation of soil erosion in
511   complex Moroccan gully morphology using structure from motion." *Remote*
512   *Sensing* 6: 7050-7080.

513   Kromer, R. A., Abellán, A., Hutchinson, D. J., Lato, M., Edwards, T., and M.
514   Jaboyedoff. 2015. "A 4D filtering and calibration technique for small-scale point
515   cloud change detection with a terrestrial laser scanner." *Remote Sensing* 7:
516   13029-13052.

517 Lague, D., Brodu, N. and J. Leroux. 2013. "Accurate 3D comparison of complex
518   topography with terrestrial laser scanner: Application to the Rangitikei canyon
519   (N-Z)." *ISPRS Journal of Photogrammetry Remote Sensing* 82: 10-26.

520 Laignel, B. 1997. "Les altérites à silex de l'ouest du Bassin de Paris: caractérisation
521   lithologique, genèse et utilisation potentielle comme granulats." PhD diss.,
522   University of Rouen.

523 Lato, M. J., Diederichs, M. S., and D. J. Hutchinson. 2010. "Bias Correction for View-
524   limited Lidar Scanning of Rock Outcrops for Structural Characterization." *Rock
525   Mechanics and Rock Engineering* 43: 615-628.

526 Laute, K., Letortu, P., Le Dantec, N. 2017. "Processes and mechanisms governing hard
527   rock cliff erosion in western Brittany, France." Poster presented at the EGU
528   General Assembly, Vienna, April 23-28.

529 Letortu, P., Costa, S., Bensaid, A., Cador, J. M., and H. Quénol. 2014. "Vitesses et
530   rythmes de recul des falaises crayeuses de Haute-Normandie (France) :
531   méthodologie et variabilité du recul." *Géomorphologie, relief, processus et
532   environnement* 2: 133-144.

533 Letortu, P., Costa, S., Cador, J. M., Coinaud, C., and O. Cantat. 2015a. "Statistical and
534   empirical analyses of the triggers of coastal chalk cliff failure." *Earth Surface
535   Processes and Landforms*, 40 (10): 1371-1386. doi: 10.1002/esp.3741

536 Letortu, P., Costa, S., Maquaire, O., Delacourt, C., Augereau, E., Davidson, R., Suanez,
537   S., and J. Nabucet. 2015b. "Retreat rates, modalities and agents responsible for
538   erosion along the coastal chalk cliffs of Upper Normandy: The contribution of
539   terrestrial laser scanning." *Geomorphology*, 245: 3-14. doi:
540   10.1016/j.geomorph.2015.05.007

541 Lichti, D., and J. Skaloud. 2010. "Registration and calibration." In *Airborne and
542   Terrestrial Laser Scanning*, edited by Vosselman G., and H. S. Maas, 83-133.
543   Whittles Publishing: Dunbeath.

544 Lim, M., Rosser, N. J., Petley, D. N., and M. Keen. 2011. "Quantifying the controls and
545   influence of tide and wave impacts on coastal rock cliff erosion." *Journal of
546   Coastal Research* 27: 46-56. doi:10.2112/JCOASTRES-D-09-00061.1

547 Medjkane, M., Maquaire, O., Costa, S., Roulland, T., Letortu, P., Fauchard, C., Antoine,
548   R., and R. Davidson. Accepted. "High resolution monitoring of complex coastal

morphology changes: Cross-efficiency of SfM and TLS based survey (Vaches-Noires cliffs, Normandy, France)." *Landslides*.

Michoud, C., Carrea, D., Costa, S., Derron, M. H., Jaboyedoff, M., Davidson, R., Delacourt, C., Letortu, P., and O. Maquaire. 2014. "Landslide detection and monitoring capability of boat-based mobile laser scanning along Dieppe coastal cliffs, Normandy." *Landslides*. doi: 10.1007/s10346-014-0542-5.

Mortimore, R. N., and A. Duperret. 2004. *Coastal chalk cliff instability*. Engineering Geology Special Publications, London.

Naylor, L. A., Stephenson, W. J., and A. S. Trenhaile. 2010. "Rock coast geomorphology: recent advances and future research directions." *Geomorphology* 114: 3-11.

Oppikofer, T., Jaboyedoff, M., Blikra, L., Derron, M. H., and R. Metzger. 2009. "Characterization and monitoring of the Åknes rockslide using terrestrial laser scanning." *Natural Hazards Earth System Sciences* 9: 1003-1009.

Pesci, A., Teza, G., and E. Bonali. 2011. "Terrestrial laser scanner resolution: numerical simulations and experiments on spatial sampling optimization." *Remote Sensing* 3: 167-184.

Pirotti, F. 2013. "State of the art of ground and aerial laser scanning technologies for high-resolution topography of the earth surface." *EuJRS* 46: 66-78.

Pomerol, B., Bailey, H. W., Monciardini, C., and R. N. Mortimore. 1987. "Lithostratigraphy and biostratigraphy of the Lewes and Seaford chalks: a link across the Anglo-Paris basin at the Turonian-Senonian boundary." *Cretaceous Research* 8: 289-304

Raber, G. T., Jensen, J. R., Hodgson, M. E., Tullis, J. A., Davis, B. A., and J. Berglund. 2007. "Impact of Lidar nominal post-spacing on DEM accuracy and flood zone delineation." *Photogrammetry Engineering Remote Sensing* 73: 793-804.

Riegl. 2014. Data sheet VZ-400. 4p

Smith, M. W., Carrivick, J. L., Hooke, J., and M. J. Kirkby. 2014. "Reconstructing Flash Flood Magnitudes Using 'Structure-from-Motion': a rapid assessment tool." *Journal of Hydrology* 519: 1914-1927.

Smith, M. W., Carrivick, J., and D. Quincey. 2016. "Structure from motion photogrammetry in physical geography." *Progress in physical geography* 40: 247-275

582 Sturzenegger, M., and D. Stead. 2009. "Quantifying discontinuity orientation and
583   persistence on high mountain rock slopes and large landslides using terrestrial
584   remote sensing techniques." *Natural Hazards Earth System Sciences* 9: 267–
585   287.

586 Su, J., and E. Bork. 2006. "Influence of vegetation, slope, and lidar sampling angle on
587   DEM accuracy." *Photogrammetry Engineering Remote Sensing* 72: 1265-1274.

588 Teza, G., Galgaro, A., Zaltron, N., and R. Genevois. 2007. "Terrestrial laser scanner to
589   detect landslide displacement fields: A new approach." *International Journal*
590   *Remote Sensing* 28: 3425-3446.

591 Vann Jones, E. C. (née Norman), Rosser, N. J., Brain, M. J., and D. N. Petley. 2015.
592   "Quantifying the environmental controls on erosion of a hard rock cliff." *Marine*
593   *Geology* 363: 230-242.

594 Westoby, M., Brasington, J., Glasser, N., Hambrey, M., and J. Reynolds. 2012.
595   ""Structure-from-Motion" photogrammetry: A low cost, effective tool for
596   geoscience applications." *Geomorphology* 179: 300-314.

597 Young, A. P., Olsen, M. J., Driscoll, N., Rick, R. E., Gutierrez, R., Guza, R. T.,
598   Johnstone, E., and F. Kuester. 2010. "Comparison of airborne and terrestrial
599   lidar estimates of seacliff erosion in Southern California*." Photogrammetric*
600   *Engineering & Remote Sensing* 76: 421–427.

601 Young, A. P. 2015. "Recent deep-seated coastal landsliding at San Onofre State Beach,
602   California." *Geomorphology* 228: 200–212.

603

604 **Tables**

Method	Number of points	Surface (m²)	Average density per m² on the cliff face	Sampling distance on cliff face for the raw point cloud
Terrestrial photogrammetry (TP)	124,757, 214	13,897	8,977	Irregular: mean of 1 point every 0.0105 m
UAV photogrammetry (UAVP)	59,418,289	15,535	3,824	Regular: mean of 1 point every 0.016 (mean)

Terrestrial laser scanning (TLS)	2,553,230	14,190	178	Irregular: mean of 1 point every 0.06 m (mean)

605 Table 1. Main characteristics of raw datasets

		TLS	TP_SF	UAVP_SF
Main characteristics	**Number of points**	2,264,742	2,030,389	2,160,790
	Mean density (per m²)	293 (±159)	183 (±17)	171 (±15)
	Density interval per m²	1-657	1-355	1-396
Advantages		Few occlusions (except caves where the TLS station is not well positioned)	Homogeneous density (less than UAVP because manual snapping is more irregular)	Homogeneous density and there are no occlusions at cliff top and cliff foot
Disadvantages		Heterogeneous density due to TLS stations and there are some occlusions due to rock fall and hollow terrain	Occlusions (overhanging areas at cliff top, rock fall at cliff foot)	

606 Table 2. Characteristics, advantages and disadvantages of the TLS, TP and UAVP point
607 clouds (after subsampling and cleaning)

	TP point cloud vs. TLS mesh		UAVP point cloud vs. TLS mesh	
	Mean error	**Standard deviation**	**Mean error**	**Standard deviation**
Whole cliff face	0.005	0.05	0.014	0.037

608 Table 3. Mean error and standard deviation values (m) between TP and UAVP whole
609 cliff-face point clouds vs. TLS mesh

	TLS (Riegl® VZ-400 or similar)	TP (Nikon D800 or similar)	UAVP (DS6 + Nikon D800 or similar)

Precision	high	low	high
Purchase and maintenance costs	very expensive (purchase: 150 k€)	cheap (purchase: 1.5 k€)	expensive (purchase: 10 k€)
Weight (instruments and targets)	very heavy (33 kg)	light (5 kg)	heavy (9 kg)
Battery life	long	very long	short
Speed of data acquisition	low	low	very high
Sensitivity to occlusion	high	high	very low
Sensitivity to bad weather (rainfall, wind)	high	very low	high
Number of man/days	high	low	high
Ability to implement survey (targets, pilot, station location)	poor	very good	good
Flexibility in the ability to capture the interest area (overhanging, caves, etc.)	low	low	very high
Level of acquisition skill needed	high	high	very high
Acquisition duration	long	long	short
Processing duration	long	very long	very long

Table 4. Summary of strengths (significant strengths in green in the online version, light gray in the print version) and weaknesses (significant weaknesses in red in the online version, dark gray in the print version) of TLS, TP and UAVP methods for Normandy cliff erosion monitoring

List of figures
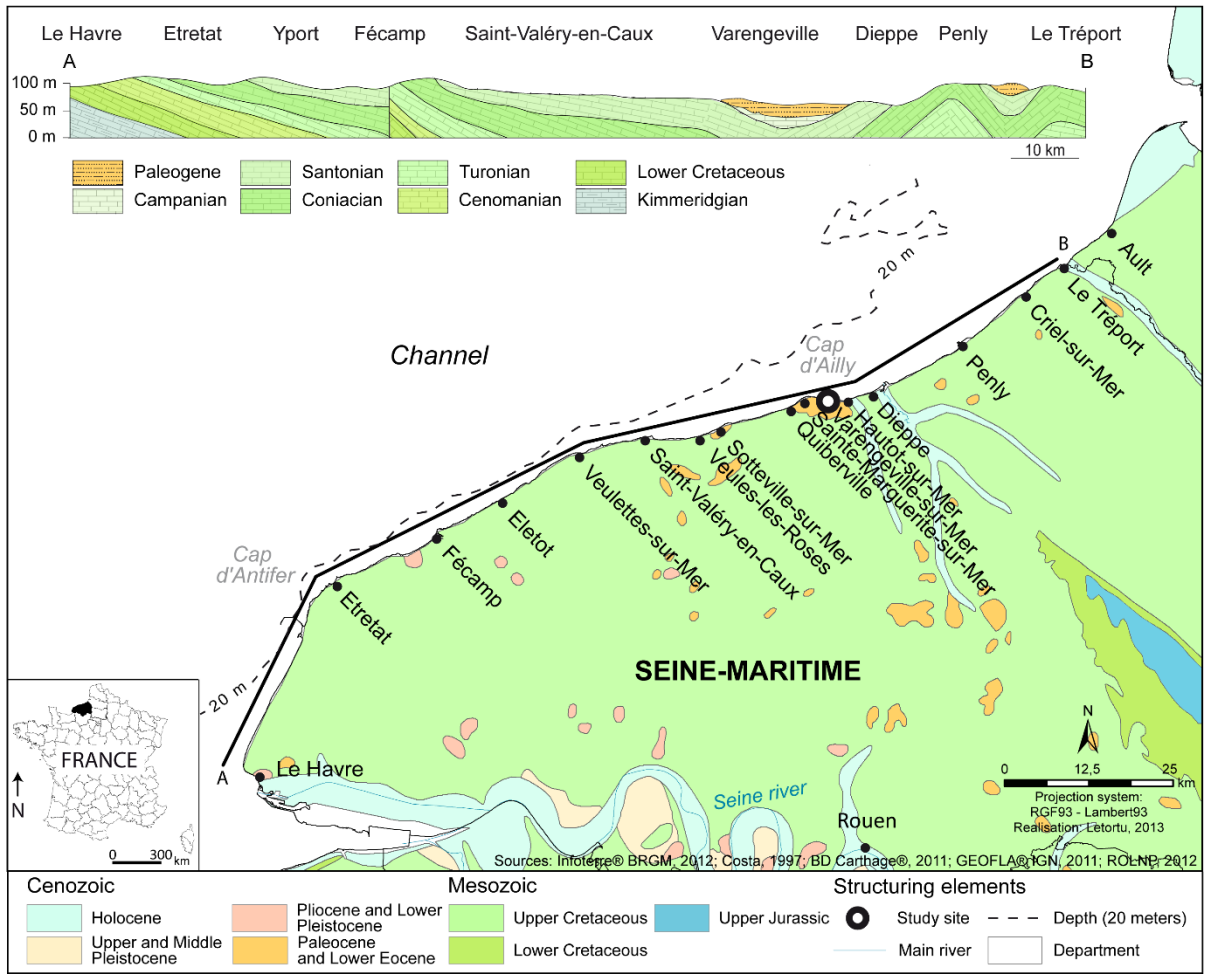
616

617   Figure 1. Presentation of the study area
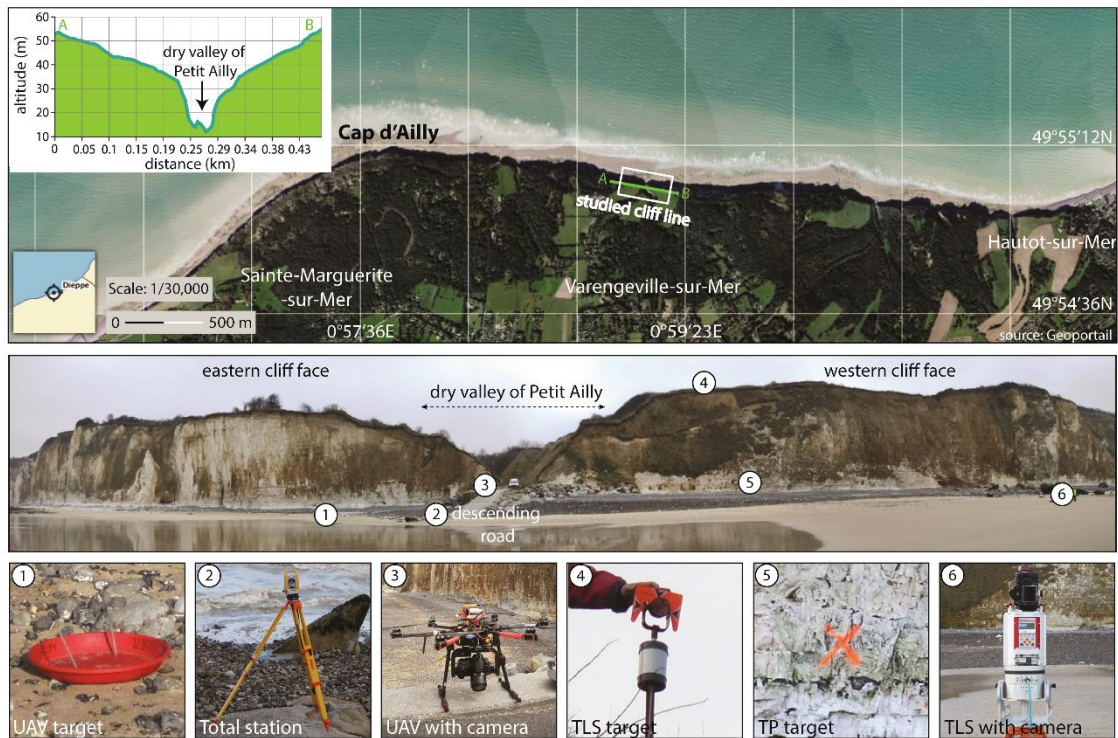
618

619   Figure 2. Panorama of Petit Ailly cliff face (Varengeville-sur-Mer) and instrumentation

620   used for the survey (28 January 2016)
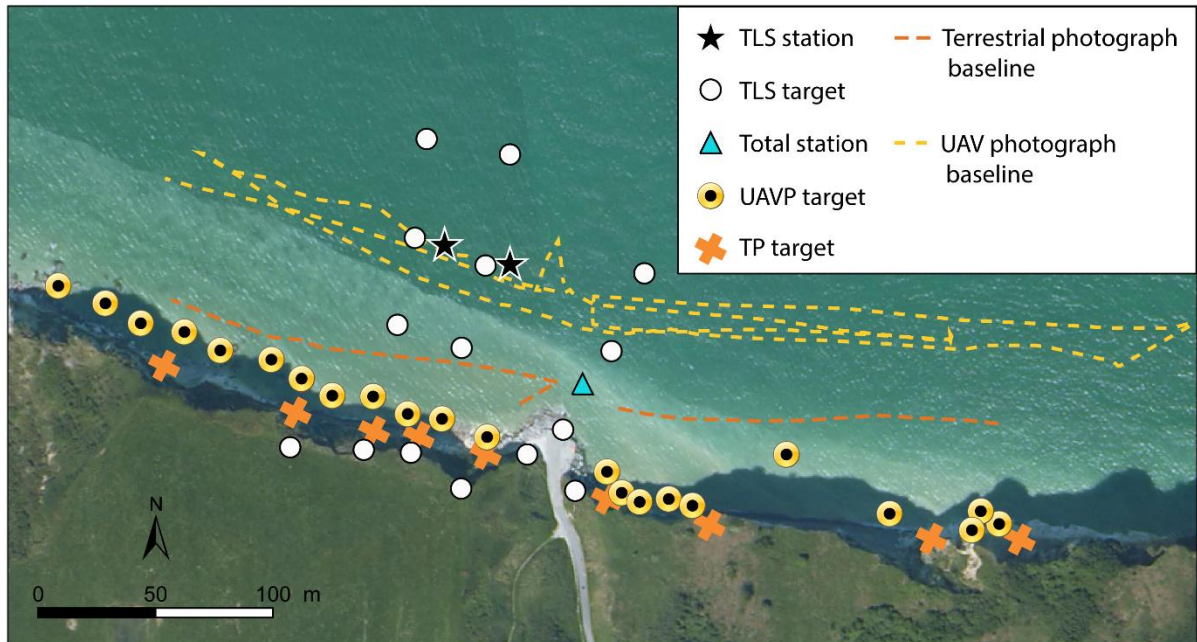
621

622   Figure 3. Location of the instruments, GCPs and protocol for the survey (28 January

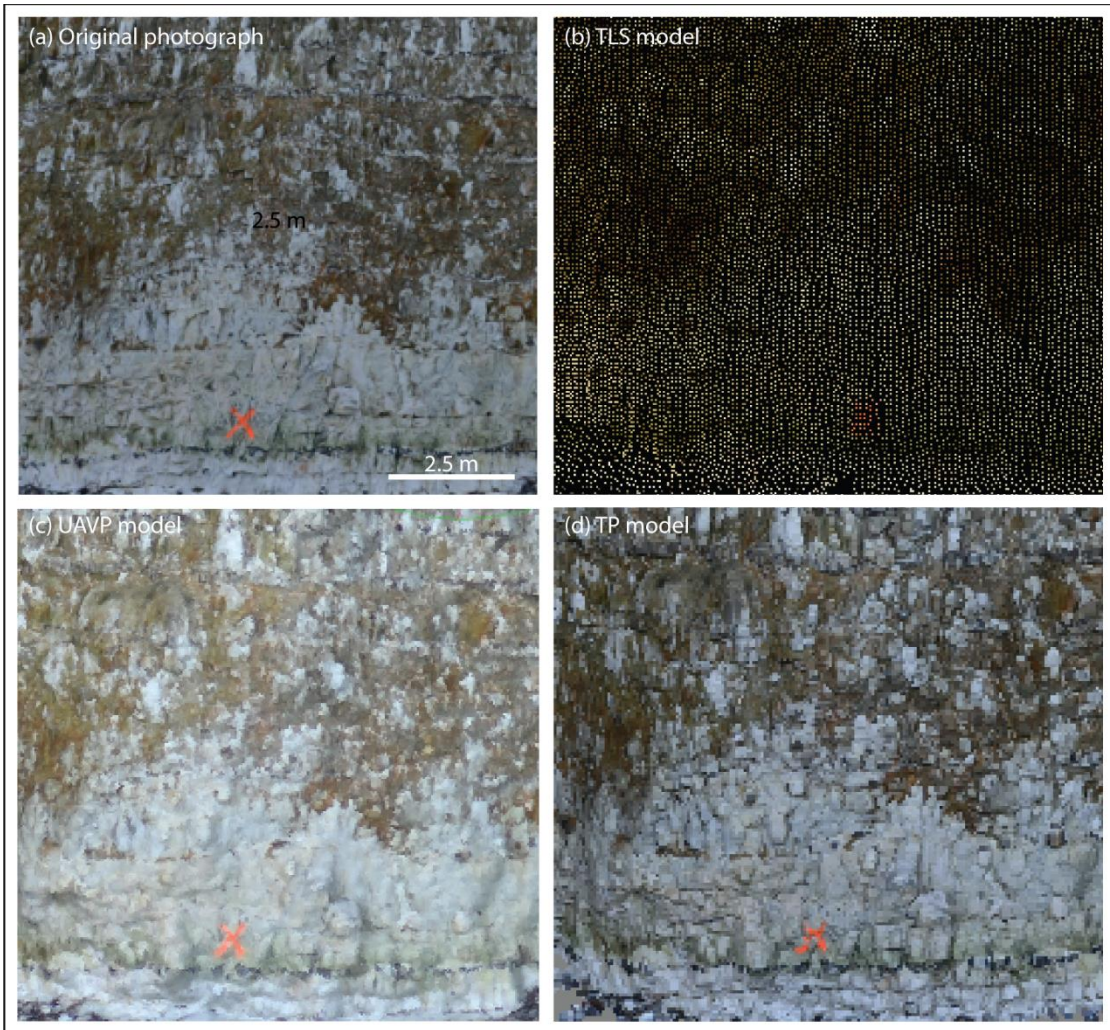623   2016) (cliff-top view)

624

28

625
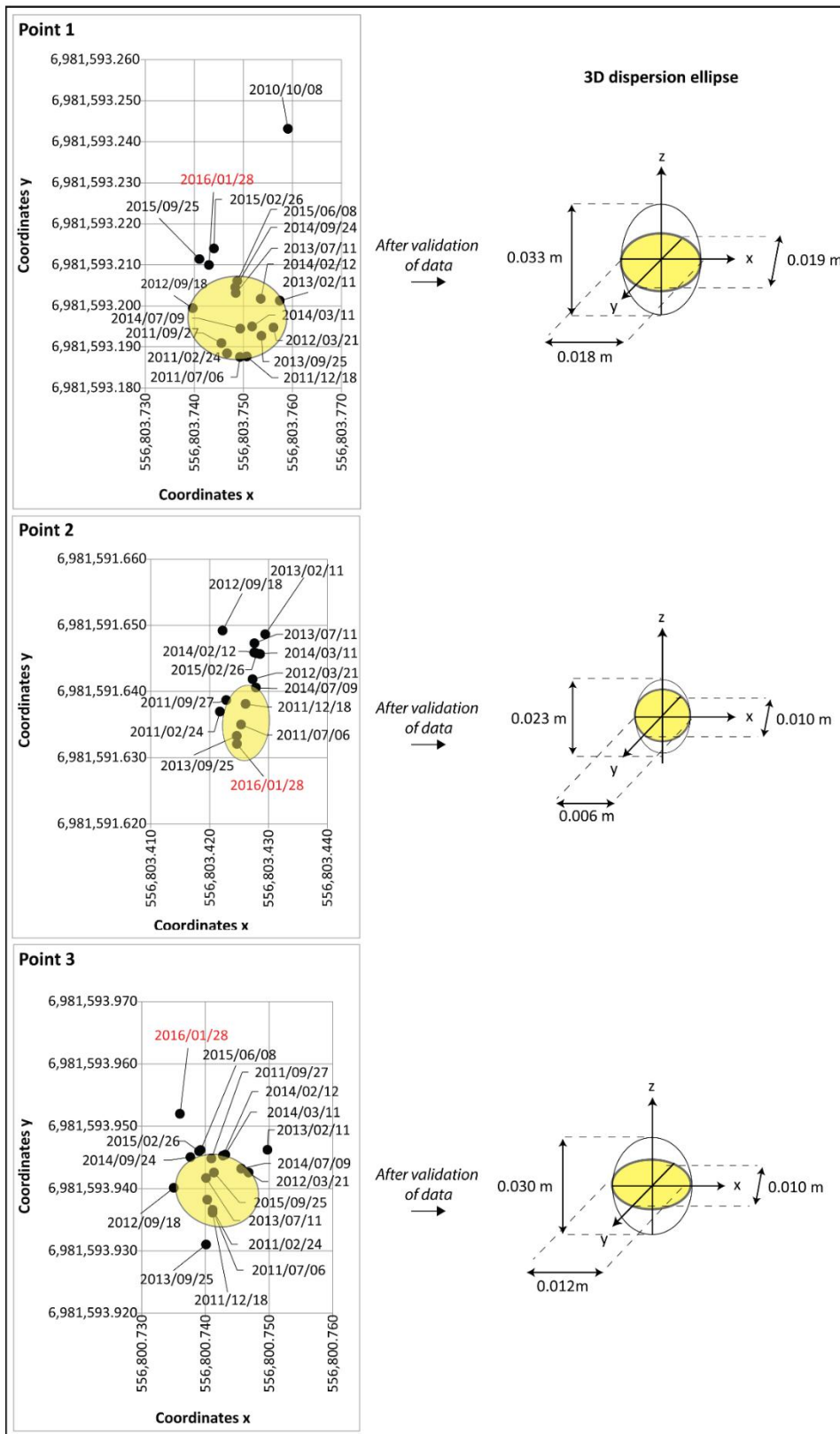
Figure 4. Maximum dispersion ellipses measured by the total station at surveyor nails
for the long-term monitoring (the survey used in this paper is depicted in orange in the
online edition)

629
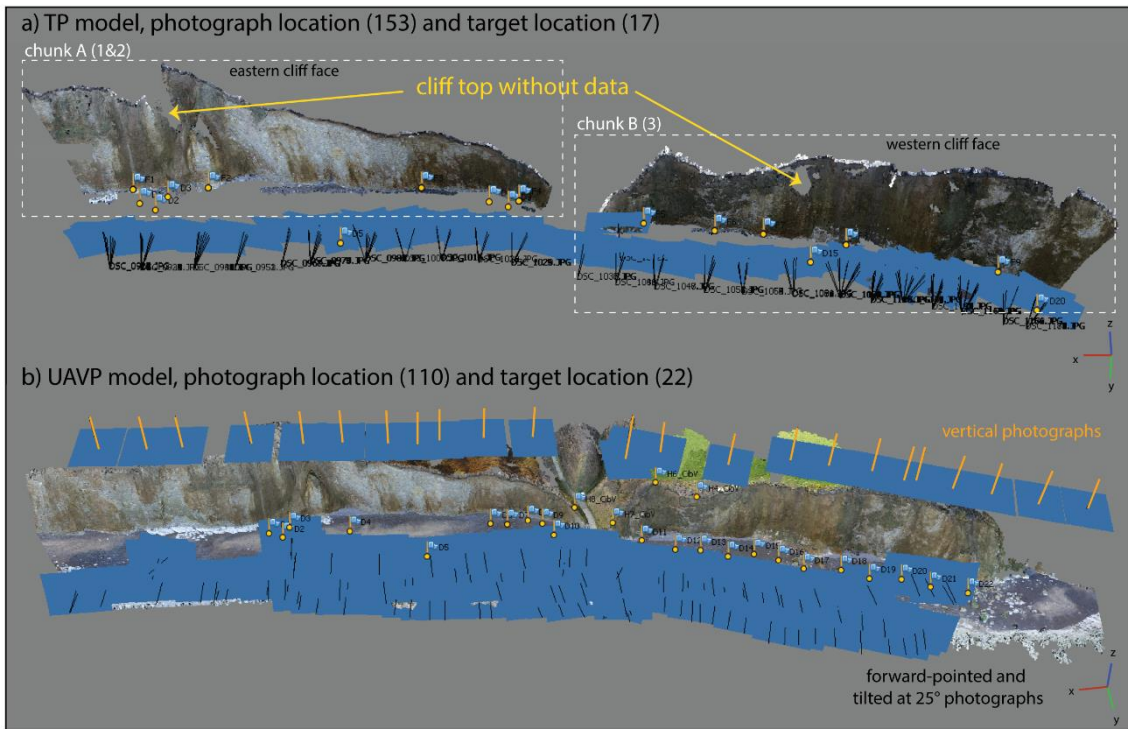
Figure 5. Location and overlap of photographs, location of GCPs, and TP and UAVP

models

632

Figure 6. Cliff face zoom from (a) original photograph, (b) TLS model, (c) UAVP
model and (d) TP model

635

31
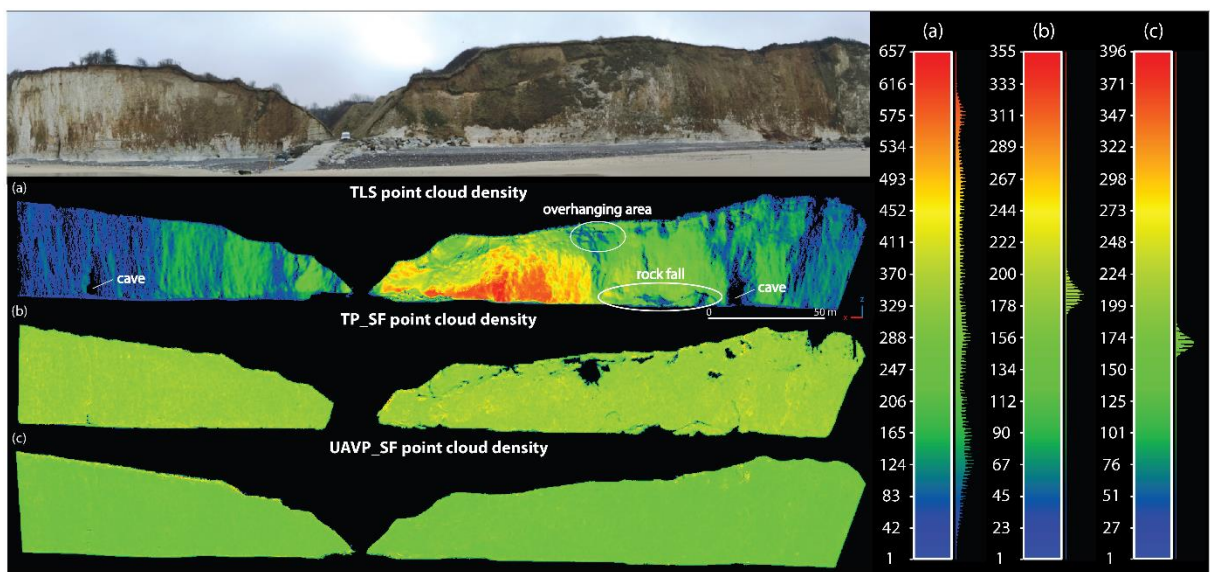
636   Figure 7. Density of point clouds per m² (TLS, TP, UAVP)
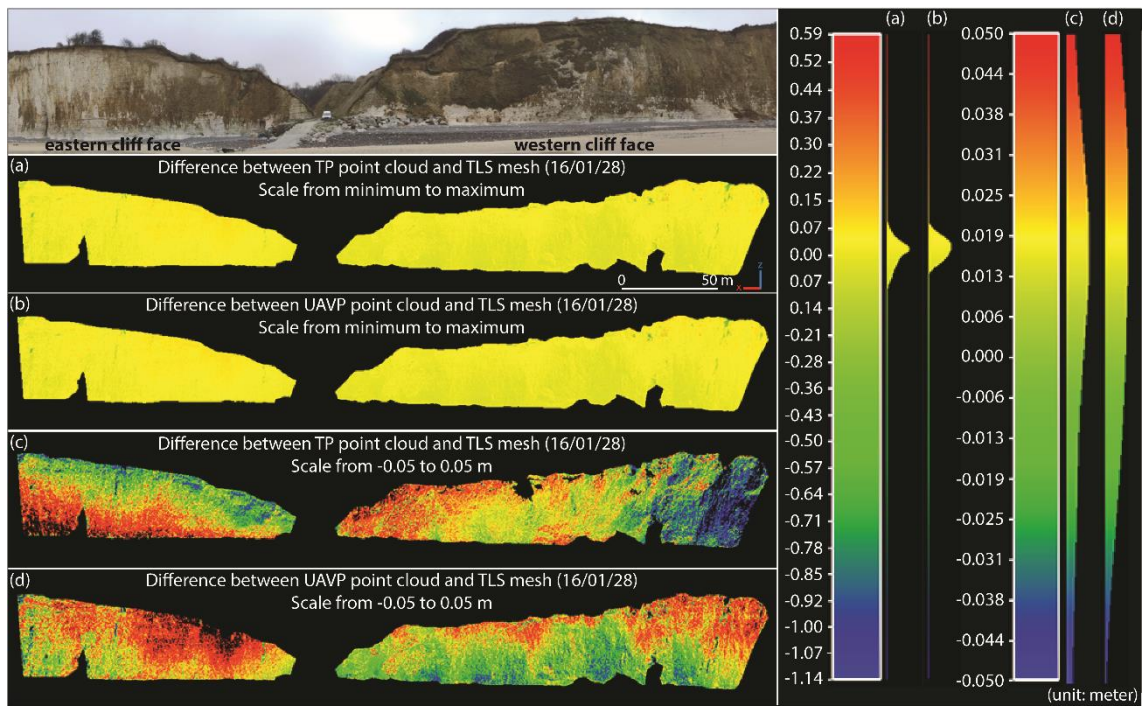
637

638   Figure 8. Distribution of difference between datasets over the cliff face

	TP point cloud vs. TLS mesh		UAVP point cloud vs. TLS mesh	
	mean error	σ	mean error	σ
All cliff face strips	0.016	0.031	0.015	0.026
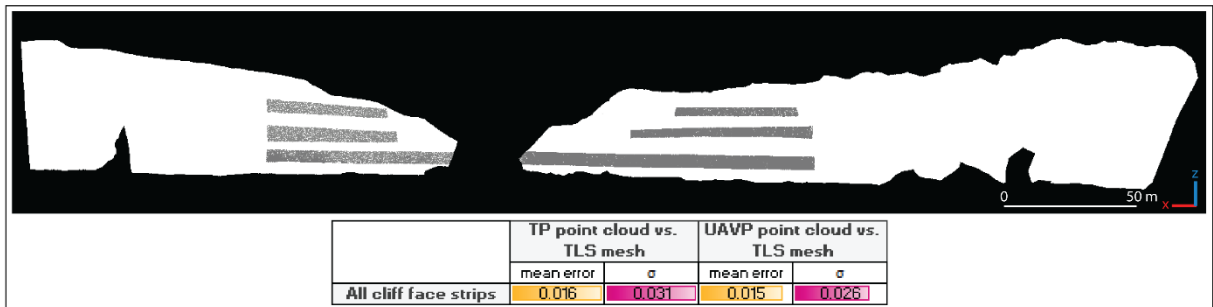
639

640   Figure 9. Comparison between all cliff-face strip error values and standard deviation

641

642